

NUMERICAL SIMULATION OF THE DYNAMICS OF RF CAPACITIVE DISCHARGE IN CARBON DIOXIDE

 V. Lisovskiy*,  S. Dudin, A. Shakhnazarian, P. Platonov,  V. Yegorenkov

V.N. Karazin Kharkiv National University, 4 Svobody Sq., Kharkiv, 61022, Ukraine

**Corresponding Author e-mail: lisovskiy@yahoo.com*

Received June 12, 2024; revised July 21; accepted August 15, 2024

In this research, the one-dimensional fluid code SIGLO-rf was used to study the internal parameters of RF capacitive discharge in carbon dioxide, focusing mainly on time-averaged and spatio-temporal distributions of discharge parameters. With the help of this code, in the range of distances between electrodes $d = 0.04 - 8$ cm, RF frequencies $f = 3.89 - 67.8$ MHz, and values of carbon dioxide pressure $p = 0.1 - 9.9$ Torr, averaged over the RF period axial profiles of the density of electrons, positive and negative ions were calculated as well as potential and electric field strength. It is shown that the discharge plasma in CO₂ contains electrons, positive ions, as well as negative ions. The negative ions of atomic oxygen are formed by the dissociative attachment of electrons to CO₂ molecules. Studies of the spatio-temporal dynamics of plasma parameters (electron density, potential and electric field strength, as well as ionization and attachment rates) in RF capacitive discharge in CO₂ showed that during half of the RF period, 1 to 3 ionization bursts are usually observed. They correspond to stochastic heating in the near-electrode sheath and the formation of passive and active double layers near the sheath boundaries. The passive double layer appears in the cathode phase and maintains the discharge plasma. The active layer is formed in the anodic phase and ensures a balance of positive and negative charges escaping to the electrode during the RF period. It was found that when the conditions $pd = 2$ Torr cm and $fd = 27.12$ MHz cm are met simultaneously, during half of the RF period, 4 intense ionization peaks are observed: resulting from stochastic heating, passive, active, and additional (auxiliary) double layers. The auxiliary double layer helps bring electrons to the surface of the temporary anode and occurs near its surface inside the near-electrode sheath. Using the similarity law, the conditions for the existence of these 4 ionization peaks in a wide range of RF frequencies, carbon dioxide pressures, and distances between electrodes were verified.

Keywords: *Radio-frequency capacitive discharge; Fluid modeling; Carbon dioxide; Ionization rate; Double layers; Negative ions*

PACS: 52.80.Pi, 52.50.Qt, 52.65.Kj

INTRODUCTION

Radiofrequency capacitively coupled gas discharge has become practically irreplaceable in many plasma technologies of micro- and nanoelectronics [1–9]. These include processes of plasma etching of semiconductor materials, deposition of various coatings from the gas phase, and many others. Therefore, the properties of the RF discharge are widely studied both experimentally [10–19] and theoretically [10, 20–29]. Numerical modeling allows us to study not only the behavior of the average plasma parameter profiles (potential, electric field, ion and electron densities, etc.) over the RF period, but also to determine their dynamics under various conditions [30–39], as well as to explain experimentally observed phenomena and predict new ones.

Radiofrequency capacitive discharge in electronegative gases turned out to be especially rich in new phenomena [16, 17, 22, 40–53]. Electronegative gases are gases whose molecules capture free electrons, forming singly charged negative ions. Their presence in a sufficiently high concentration in a gas mixture significantly changes the charged particle generation and loss processes in the discharge plasma. The rate of ambipolar losses decreases [42, 44, 46], up to the transition of ambipolar diffusion to free diffusion [47]. Accordingly, this affects the time-averaged plasma potential and the flow of positive ions from the plasma to the electrodes [40, 41]. Due to the retention of negative ions in the average potential well in the RF capacitive discharge, their density increases. In this case, it can exceed the electron concentration by tens to hundreds (and sometimes thousands) times, and the plasma consists of positive and negative ions in approximately equal concentrations with a small addition of free electrons [41, 42, 44, 46]. At certain moments of the RF period, double layers of space charge may appear in the discharge [44, 54–58]. The enhanced electric field of the double layer leads to ionization bursts, which allows maintaining stable discharge operation. We will consider this problem in more detail below.

In addition, the RF capacitive discharge is widely used in pumping CO₂ gas lasers [59–62]. Recently, a separate line of research has actually formed, dedicated to the plasma conversion of carbon dioxide [63–76]. These studies aim to solve the problem of the greenhouse effect associated with emissions of carbon dioxide into the atmosphere formed during the combustion of fossil fuels. The researchers are seeking an efficient method of splitting CO₂ molecules into carbon monoxide and oxygen, which can be used both in terrestrial conditions and to provide future colonies on Mars with fuel and oxygen. In this case, high values of the conversion coefficient of CO₂ molecules can be achieved in the plasma of the RF capacitive discharge [65–70]. However, the conversion process in such a discharge is quite complicated and not well understood due to the high level of spatial inhomogeneity of the discharge plasma and the significant and fast change of plasma parameters distribution during the RF period.

In this paper, the dynamics of processes in a RF capacitive discharge in carbon dioxide is investigated using the SIGLO-rf fluid code. Particular attention is paid to the mechanisms of direct ionization of CO₂ molecules by electron impact, and the clarification of the reasons for their appearance in certain places of the discharge at certain moments of the RF electric field period. The appearance of intense ionization in a certain part of the discharge should be accompanied by increased dissociation of CO₂ molecules, which is of interest for solving the problem of plasma conversion of carbon dioxide.

SIGLO-RF CODE DESCRIPTION

1D fluid code SIGLO-rf is the software intended for simulation of RF capacitively coupled discharge. It is based on the equations and assumptions given in the papers of Prof. J.-P. Boeuf and Prof. L.C. Pitchford [56,58] and was developed at the University of Toulouse.

SIGLO-rf allows self-consistent calculation of temporal and average axial profiles of the density of charged particles (electrons, positive and negative ions), as well as potential and electric field strength over the RF period. In addition, it is possible to determine the density of the discharge current (electrons and ions both in the plasma and on the electrode, full current, displacement current), the power absorbed by ions and electrons, the electron temperature T_e , etc. At the same time, SIGLO-rf numerically integrates the system of balance equations for electrons, positive and negative ions, as well as Poisson's equation. Calculations are carried out from the initial value of the density of charged particles, which can be changed before starting the calculations, until a periodic steady state is reached. At the very beginning, the type and pressure of the gas p , the frequency of the RF electric field f , the distance between the electrodes d , and the gas temperature T_g are defined. Ion-induced electron emission is not taken into account, the corresponding coefficient $\gamma = 0$. That is, the SIGLO-rf code can be used only for calculations of the low-current α -mode of the RF capacitive discharge. At the same time, it is considered that 25% of electrons are reflected from the surface of the electrodes.

The input file with the gas parameters must contain the dependences of the average electron energy ε , their mobility μ_e , the ionization coefficient $\alpha = v_i/(\mu_e E)$, and the electron attachment coefficient $\eta = v_a/(\mu_e E)$, as a function of the reduced electric field E/p at a gas temperature of 300 K. Next, the SIGLO-rf code determines the dependences of the electron mobility μ_e , the ionization frequency v_i , the attachment frequency v_a , the energy loss frequency, and the diffusion coefficient D_e (which is determined using the Einstein's relation) on the average electron energy ε . Additionally, it is assumed that μ_e , D_e , v_i and v_a depend on the local average electron energy $\varepsilon(x,t)$ in the same way as under equilibrium conditions.

The input file should also contain the dependence of ion mobility on the local reduced electric field E/p . The diffusion coefficient of ions (both positive D_p and negative D_n) is determined from Einstein's relation at a weak field and is considered constant.

The densities of electrons n_e , positive n_p and negative ions n_n , the average electron energy ε and the potential V distribution are determined using the following equations. First, the balance equation for the density (continuity equation) is used for electrons:

$$\frac{\partial n_e}{\partial t} + \frac{\partial}{\partial x} \Phi_e = S_e, \quad (1)$$

where

$$S_e = (v_i - v_a)n_e + v_{detach}n_n - k_{recomb(e-i)}n_en_p. \quad (2)$$

It can be seen from equation (2) that the detachment of electrons from negative ions with the frequency v_{detach} is taken into account, and the coefficient $k_{recomb(e-i)}$ describes the loss of electrons during their recombination with positive ions.

Secondly, flow equations are also used to describe electrons

$$\Phi_e = -e\mu_e E n_e - D_e \frac{\partial n_e}{\partial x} \quad (3)$$

as well as the energy balance equation

$$\frac{\partial (n_e \varepsilon)}{\partial t} + \frac{5}{3} \frac{\partial}{\partial x} \Phi_\varepsilon = S_\varepsilon. \quad (4)$$

As already mentioned above, the dependence of the electron diffusion coefficient D_e on the average energy ε is found using the Einstein relation,

$$\frac{D_e}{\mu_e} = \frac{k_B T_e}{e} = \frac{2}{3} \frac{\varepsilon}{e}, \quad (5)$$

where k_B is Boltzmann constant, e is elementary charge.

The energy flux Φ_ε in equation (4) is defined as

$$\Phi_\varepsilon = -n_e \varepsilon \mu_e E - D_e \frac{\partial}{\partial x} (n_e \varepsilon). \quad (6)$$

The right-hand side of equation (4) contains

$$S_\varepsilon = -e\Phi_e E - n_e L(\varepsilon). \quad (7)$$

Here, the energy loss term $L(\varepsilon) = e\mu_e E^2$ is assumed to be the same as under equilibrium conditions (where $S_\varepsilon = 0$).
For positive ions, the balance (continuity) equation is solved:

$$\frac{\partial n_p}{\partial t} + \frac{\partial}{\partial x} \Phi_p = S_p, \quad (8)$$

where

$$S_p = \nu_i n_e - k_{recomb(e-i)} n_e n_p - k_{recomb(i-i)} n_n n_p. \quad (9)$$

The coefficient $k_{recomb(i-i)}$ takes into account the process of ion-ion recombination, that is, the loss of positive ions due to their recombination with negative ions. In equation (8), the flow of positive ions

$$\Phi_p = +e\mu_p E n_p - D_p \frac{\partial n_p}{\partial x} \quad (10)$$

where μ_p and D_p are mobility and diffusion coefficient of positive ions, respectively.

Similarly, the balance (continuity) equation is solved for negative ions:

$$\frac{\partial n_n}{\partial t} + \frac{\partial}{\partial x} \Phi_n = S_n, \quad (11)$$

where

$$S_n = \nu_a n_e - k_{recomb(i-i)} n_n n_p - \nu_d n_n. \quad (12)$$

Here it is taken into account that negative ions can be lost not only during ion-ion recombination but also when electrons are detached from them with frequency ν_d . Recall that negative ions are formed with a frequency of ν_a as a result of free electron attachment to the molecules of an electronegative gas.

The flux of negative ions is described by the formula

$$\Phi_n = -e\mu_n E n_n - D_n \frac{\partial n_n}{\partial x}, \quad (13)$$

where μ_n is mobility of negative ions, D_n is their diffusion coefficient.

Poisson's equation for the electric potential should be added to the above fluid equations

$$\frac{\partial^2 V}{\partial x^2} = -\frac{e}{\varepsilon_0} (n_p - n_e - n_n). \quad (14)$$

At the same time, the potential is related to the electric field E by the equation

$$E = -\frac{\partial V}{\partial x}. \quad (15)$$

Now consider the boundary conditions. For the fluxes or densities of charged particles on the electrodes, they were as follows. The electron flux is equal to the thermal flow $n_e v_{the}/4$, where v_{the} is the thermal velocity of electrons. The ion density on the electrode is zero. Taking into account the small diffusion coefficient of ions, this means that their flow is equal to the drift flow when the ion velocity is directed towards the electrode. Otherwise, the ion flux is zero. We have already noted above that the reflection coefficient of electrons from the surface of the electrodes does not depend on their energy and is equal to 25%.

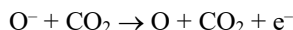
In addition, we consider the left electrode to be grounded ($V(0) = 0$), and the voltage from the RF generator with the waveform $V(d) = V_{rf} \cos(\omega t)$ is applied to the right electrode.

Calculations are made for carbon dioxide. Preliminary, the dependences of the electron mobility μ_e , the average electron energy ε , the ionization coefficient (the first Townsend coefficient α/p) and the attachment coefficient η/p on the reduced electric field E/p . At the same time, cross sections of electron collisions with carbon dioxide molecules were used, given in the LXCat database (www.lxcat.net) [78], where the cross sections from the Itikawa set [79] were chosen for CO₂. In addition, the values of electron mobility in CO₂ given in [80] were used.

For CO₂, the mobility of positive CO₂⁺ ions in its own gas was taken from [81, 82], for the mobility of negative ions, the results of [81, 83] were used. The coefficient of recombination of positive and negative ions of $2 \cdot 10^{-7}$ cm³/sec was taken from [84]. Coefficient of ion-electron dissociative recombination



for cold electrons (300 K) is given in the paper [85]. Consider that this coefficient decreases with increasing electron temperature [86]. Then, for electron temperatures of several eV, this coefficient should be equal to $3.8 \cdot 10^{-8}$ cm³/sec. To take into account the process of detachment of electrons from negative ions

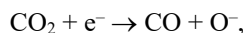


we used the dependence of the detachment coefficient on the reduced electric field given in [87].

SIMULATION RESULTS

Now let's consider the results of calculating the parameters of the RF capacitive discharge in CO₂, obtained using the SIGLO-rf code.

Carbon dioxide is one of the so-called "electronegative" gases. Collision of an electron with an energy higher than 3.3 eV [79] with a carbon dioxide molecule can lead to dissociative attachment



as a result of which a negative atomic ion of oxygen is formed. The attachment process worsens the conditions for maintaining the discharge. Free electrons can acquire high energy from the electric field and ionize gas molecules (that is, create new charged particles instead of those lost in the plasma volume, on the electrodes and walls of the discharge chamber), and must also carry the discharge current. An atom or gas molecule to which an electron has attached becomes a negative ion, the mass of which is thousands of times greater than the mass of the electron. Such an ion is not able to acquire high energy in the discharge to ionize gas molecules. Also, due to its inertness, it can carry only a small part of the discharge current. Therefore, the electrons lost due to attachment must be compensated in ionization processes.

Therefore, positive ions CO₂⁺, electrons, and negative ions O⁻ should be present in the quasi-neutral plasma of the RF discharge in carbon dioxide (see Fig.1). At the same time, to fulfill the condition of quasi-neutrality, the positive ion density must be equal to the sum of the densities of electrons and negative ions, i.e. $n_p = n_e + n_n$. So, from Figure 1 we have, firstly, that in the center of the discharge $n_p = 4.52 \cdot 10^{10} \text{ cm}^{-3}$, $n_n = 4.3 \cdot 10^{10} \text{ cm}^{-3}$, $n_e = 2.2 \cdot 10^9 \text{ cm}^{-3}$, so the quasi-neutrality is indeed fulfilled. Secondly, the negative ion density is about 20 times greater than the electron density. In fact, in the central part of the discharge, we have an ion-ion plasma with a small admixture of free electrons. However, in the near-electrode layers, the electron density is significantly higher than the negative ion density. It should be noted that electrons fill the near-electrode layers gradually, and are present there only during some part of the RF period [14,20,21]. At the same time, the closer to the electrodes, the shorter the time the electrons stay there. Therefore, the time-averaged electron density n_e in Figure 1 is much smaller than the positive ion density. But below we will see that when the near-electrode sheath adjacent to the temporary anode is filled, the electron density will be practically the same in the layer as the positive ion density.

Now consider negative ions. The high density of negative ions in the discharge is explained by the fact that the time-averaged potential of quasi-neutral plasma of the RF discharge in CO₂ is always positive (see Fig. 2). This leads to the retention of negative ions in the plasma volume, these ions cannot get to the electrodes. Negative ion density is regulated by the balance between their appearance as a result of attachment and losses due to detachment and ion-ion recombination. These listed loss processes are not fast, due to which the concentration of negative ions in the plasma can be quite large. Accordingly, the accumulation of negative ions in the plasma, firstly, reduces the ambipolar losses of positive ions [46,47], and secondly, it reduces the average plasma potential. The value of this potential (207 V) is lower than the average plasma potential in argon (230 V [88]).

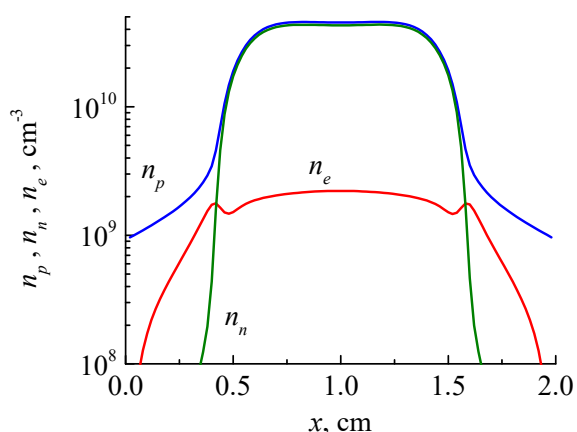


Figure 1. Time-averaged axial profiles of the density of electrons, negative and positive ions. RF discharge in CO₂ at gas pressure $p = 1$ Torr, frequency $f = 13.56$ MHz, distance between electrodes $d = 2$ cm, RF voltage amplitude $U_{rf} = 500$ V.

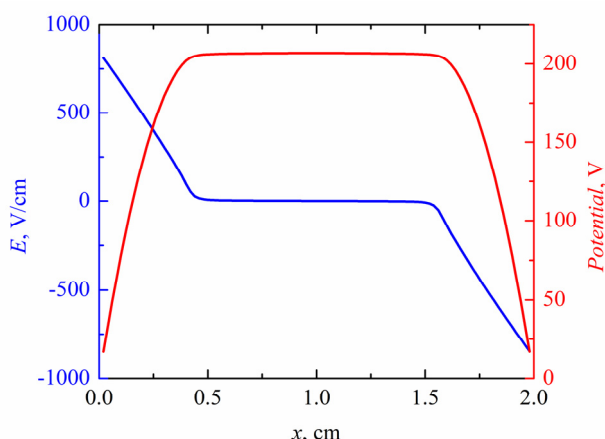


Figure 2. Time-averaged axial profiles of potential and electric field strength. RF capacitive discharge in CO₂. $p = 1$ Torr, $f = 13.56$ MHz, $d = 2$ cm, $U_{rf} = 500$ V

The RF discharge in CO₂ has a greater thickness of the near-electrode sheath (approximately 4.5 mm) than in argon under the same conditions (3 mm [88]). Therefore, the RF field strength near the electrode surface in CO₂ is significantly lower, it approaches 850 V/cm (compared to 1400 V/cm for argon).

The time-averaged electron energy (see Fig. 3) in the quasi-neutral plasma of RF discharge in CO₂ (approximately 3.5 eV) is significantly lower than for argon (reaches 6 eV [88]). The ionization rate, shown in Fig. 3, has two double maxima, which indicates the presence of an additional charged particle bearing process in the RF discharge in CO₂ compared to argon [88]. Below we will consider it in detail.

Regarding the average electron energy, we note that its value of 3.5 eV indicates that the main contribution to the CO₂ conversion process under the conditions considered in Figures 1–3 ($p = 1$ Torr, $U_{rf} = 500$ V) is not the direct dissociation of molecules by electron impact, but “climbing the ladder” of vibrational levels of molecules followed by their decomposition into CO and O [65,66, 89,90]. Electrons excite vibrational levels of CO₂ molecules, which then exchange the vibrational energy, and some part of CO₂ molecules can get enough vibrational energy to reach the dissociation threshold.

Now consider the dynamics of the plasma parameters, namely the change of their axial profiles over time. Fig. 4 shows the axial profiles of potential for several moments of the RF period.

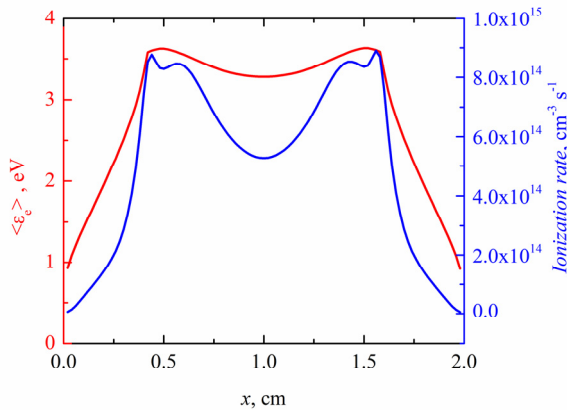


Figure 3. Time-averaged axial profiles of average electron energy and ionization rate. RF capacitive discharge in CO₂. $p = 1$ Torr, $f = 13.56$ MHz, $d = 2$ cm, $U_{rf} = 500$ V

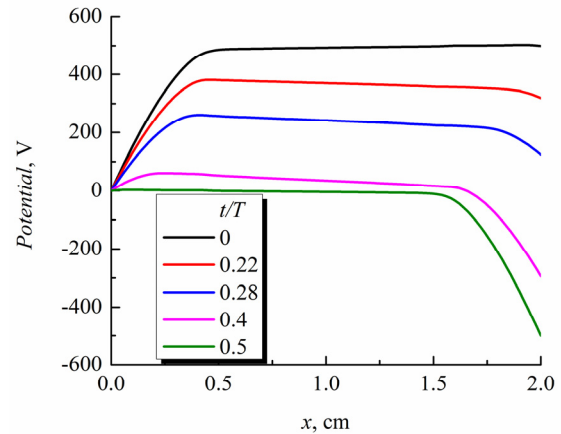


Figure 4. Axial profiles of potential for different parts of the RF period. RF capacitive discharge in CO₂. $p = 1$ Torr, $f = 13.56$ MHz, $d = 2$ cm, $U_{rf} = 500$ V

At first glance, these profiles are similar to the corresponding profiles for argon [88]. However, in the quasi-neutral plasma, the slope of the profiles in CO₂ is greater, which indicates a higher RF electric field strength. In addition, near the boundary of the collapsing near-electrode layer, the potential increases faster than in the plasma, and a so-called “double layer” is formed [41, 44, 54–58]. This is best seen on the axial profile of the electric field strength, one of which is shown in Fig. 5. In fact, the so-called “passive” (DL_1) and “active” (DL_2) double layers (by the definition in [41]) can be seen on this axial profile. Note that an additional third double layer (DL_3) began to appear in Figure 3, the presence of which is not mentioned in the papers of other authors. The role of these double layers, the conditions and causes of their occurrence will be considered below.

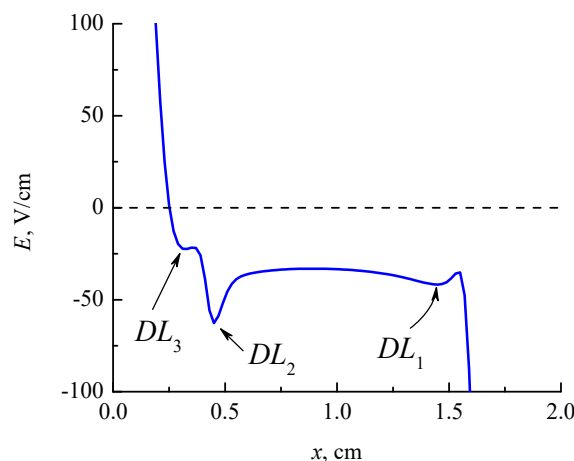


Figure 5. Axial profile of the electric field strength for the moment of the RF period $t/T = 0.4$. RF capacitive discharge in CO₂. “DL” stands for double layer. $p = 1$ Torr, $f = 13.56$ MHz, $d = 2$ cm, $U_{rf} = 500$ V

Figure 5 shows that in the central region of the plasma the field is approximately equal to 33 V/cm, and in the “active” double layer it reaches 63 V/cm. Due to the exponential dependence of the ionization frequency on the electric field strength, the ionization rate in the double layer (with approximately twice the electric field strength) should be two dozen times higher than in the plasma volume.

Let's find out why these double layers are needed in RF capacitive discharge in CO₂. To do this, first consider the dynamics of the electron density shown in Fig. 6. The densities of positive and negative ions practically do not change during the RF period, so here we give them only for the initial moment $t/T = 0$. At this moment, the electrons are completely pushed out of the left near-electrode sheath by a strong electric field, fill the right sheath, and partially hit the right electrode, which is a temporary anode. At the same time, on the corresponding profile in Fig.6 near the boundary of the right sheath (approximately at $x = 1.6$ cm), we can see a spike in the electron density, in which n_e is even higher than in the central region of the discharge.

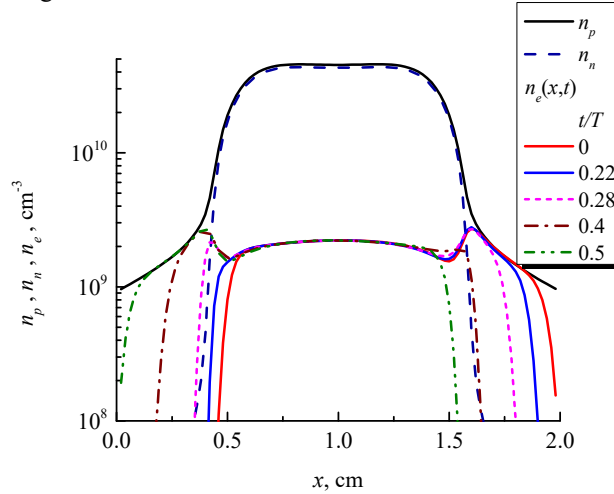


Figure 6. Axial density profiles of positive ions, negative ions and electrons for different parts of the RF period. RF capacitive discharge in CO₂. $p = 1$ Torr, $f = 13.56$ MHz, $d = 2$ cm, $U_{rf} = 500$ V

The electron density peak appeared due to the formation of an "active" double layer near the boundary of the right sheath during the previous half of the RF period. This double layer should, firstly, approximate the density of electrons and positive ions in the sheath to ensure quasi-neutrality, and secondly, bring to the right electrode the number of electrons necessary to maintain the balance of the positive and negative charges throughout the RF period. This balance must be fulfilled to ensure the stability of the discharge. But only positive ions and electrons in equal quantities can enter the electrode, while the flow of negative ions to the electrode is zero (see Fig. 7).

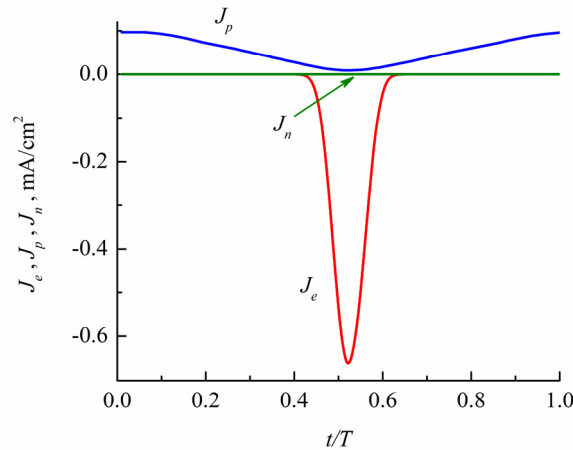


Figure 7. Time dependence of the current density of positive J_p and negative ions J_n , as well as electrons J_e on the left electrode. $p = 1$ Torr, $f = 13.56$ MHz, $d = 2$ cm, $U_{rf} = 500$ V

In the RF discharge in argon [88], where the concentrations of positive ions and electrons in a quasi-neutral plasma were equal, there were no problems with ensuring the balance of charge flows to the electrodes. However, in the CO₂ case, the electron density is approximately 20 times lower than that of positive ions. Therefore, for the required number of electrons to enter the electrode, it must be generated as a result of increased ionization. Electrons born in the plasma may not reach the electrode and stick to the gas molecules. Thus, the additional electron generation should appear just in the sheath, if possible, near the electrode. This is the reason for the formation of an "active" double layer with an increased RF electric field near the boundary of the near-electrode sheath.

Note that the presence of a maximum electron density in the region of the active double layer near the boundary of the near-electrode sheath plays an important role. When the corresponding sheath borders the temporary anode, i.e. is in the anodic phase, the electric field attracts electrons to this electrode. But from Figures 5 and 8, we see that closer to the

temporary anode, the electric field changes its sign and pushes electrons away from it. Therefore, the electrons density between the double layer and the point of the electric field sign-change increases due to their accumulation in this area. Some of the electrons pass through the potential barrier, and some are reflected back. The electron density increase leads to an increase in the diffusion current towards the temporary anode, as well as a decrease in the height of the potential barrier. Thanks to this, the necessary number of electrons can reach the temporary anode, which allows for maintaining the charge balance during the RF period.

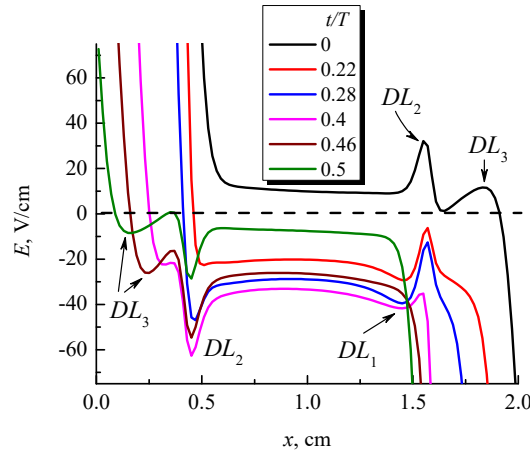


Figure 8. Axial profiles of the electric field strength for different moments of the RF period t/T . $p = 1$ Torr, $f = 13.56$ MHz, $d = 2$ cm, $U_{rf} = 500$ V

While the active double layer ensures the balance of the number of charges on the temporary anode, a "passive" double layer is also observed near the border of the opposite near-electrode sheath that is in the cathodic phase. It maintains the electron density in the plasma at a level sufficient for stable burning of the discharge, when ionization compensates for all electron losses. The electric field in the plasma volume is weaker than in the passive double layer and mainly transfers the discharge current through the plasma.

Now let's consider the reasons for the formation of the third double layer (in Figures 5 and 8 it is marked as DL_3). The thickness of the near-electrode sheath is a complex function of the frequency and amplitude of the RF voltage, the gas pressure, the electric field strength in the plasma volume, and the distance between the electrodes [2], and this is valid for electropositive gases. In electronegative gases, this dependence is even more complicated. We said above that the active double layer is formed near the boundary of the near-electrode sheath, which is in the anodic phase. Electrons born in it move towards the temporary anode. However, it is necessary to consider the process of their loss due to attachment to gas molecules. Suppose these losses are high enough so that fewer electrons pass through the near-electrode layer to the electrode than is necessary to balance the charge on its surface. In that case, another double layer is formed closer to the surface of the temporary anode, which is auxiliary and keeps the ionization rate higher than the attachment rate.

Let's return to the density profiles in Fig. 6. We considered only the profile for the initial moment $t/T = 0$. Recall that at this moment a positive amplitude value of the RF voltage (+500 V) is applied to the right electrode.

Next, the voltage on the right electrode decreases, and the potential difference between the electrode and the plasma increases (which we have already seen in Fig. 4). As a result, the thickness of the right sheath increases, and its border begins to move away from the electrode. Accordingly, the electrons that previously filled the right layer began to be pushed out of it. Electron density profiles move away from the right electrode.

In the case of low gas pressure, when electrons rarely collide with gas molecules, the reflection of electrons from the boundary of the expanding near-electrode layer plays a significant role in maintaining the discharge, and it is called "stochastic heating" [1, 4, 27]. Fluid modeling cannot describe the process of stochastic heating due to its non-local nature, but we consider here only the case of higher pressure. Electrons that filled the near-electrode layer during the anodic phase are pushed into the plasma by the electric field of the layer during the transition to the cathodic phase. However, the frequent collisions of electrons with gas molecules make it possible to describe this process using a fluid code. The term "wave-riding" electron heating is sometimes used in the literature just for the process of electron heating in the cathode phase of the near-electrode sheath [57]. But usually, this heating is also called stochastic. We will continue to use this name as well, but with the above in mind.

Due to stochastic heating of electrons a spike in the ionization rate appears in Fig. 9 in the right sheath and near its boundary (in the figure it is marked as StH - "Stochastic Heating"). After a time of approximately $t/T = 0.2$, a passive double layer (marked in Figure 9 as DL_1 - "Double Layer") appears near the border of the expanding near-electrode sheath, and after $t/T = 0.25$, near the border of the left sheath, an active double layer (DL_2) is formed. Thanks to the increased ionization rate in it, electrons gradually fill the left near-electrode layer, maintain quasi-neutrality in the filled part, and then partially escape to the left electrode to ensure the balance of the charge of the opposite sign. At $t/T = 0.4$, the formation of the third double layer (DL_3) is observed. The corresponding behavior of the electric field strength is

visible in Fig. 8. Later, at $t/T > 0.5$, stochastic heating and a double layer are formed in the reverse order, which we can see in Fig. 9. Note that approximately in the place where there was an active double layer with the maximum electric field strength, then a region with a minimum field appears since a high level of ionization is maintained due to stochastic heating (deeper in the sheath) and in the passive double layer, which is further from the electrode, deeper in the plasma volume.

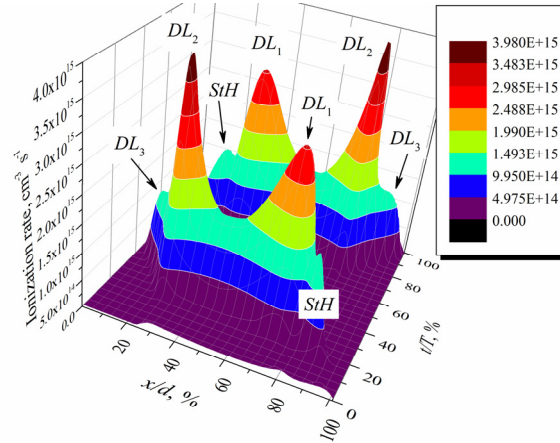


Figure 9. Space-time dependence of the ionization rate. Peaks corresponding to stochastic heating (StH) and the formation of double layers (DL) are marked. $p = 1$ Torr, $f = 13.56$ MHz, $d = 2$ cm, $U_{rf} = 500$ V

Now let's find out how the RF voltage amplitude under fixed other conditions affects the ionization processes in the discharge during the RF period. The corresponding space-time dependencies are shown in **Fig. 10**.

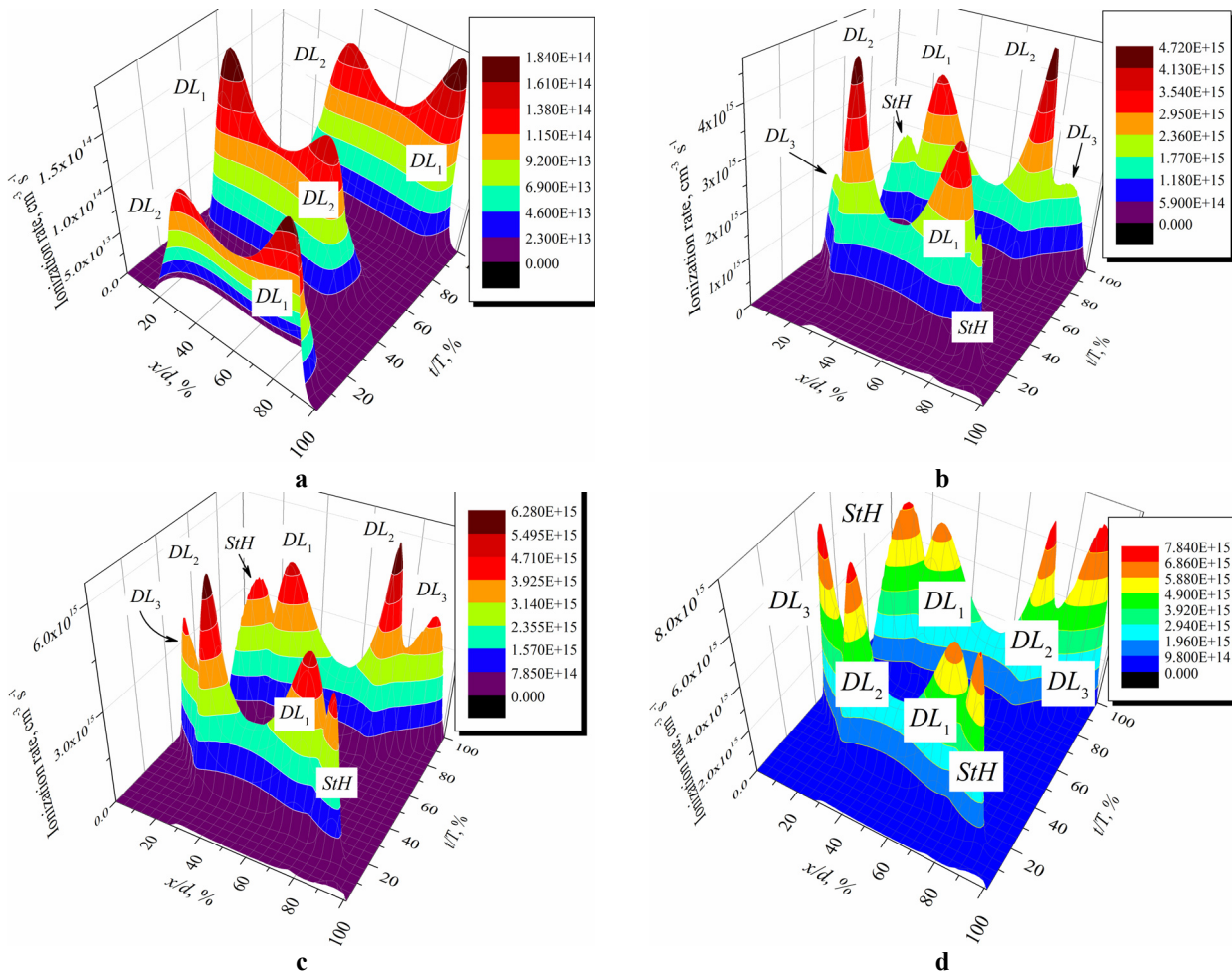


Figure 10. Space-time dependence of the ionization rate. $p = 1$ Torr, $f = 13.56$ MHz, $d = 2$ cm, $U_{rf} =$ a) 85 V, b) 600 V, c) 800 V, d) 1000 V

At the lowest RF voltage (85 V at a pressure of 1 Torr), we see only two peaks corresponding to the passive (DL_1) and active (DL_2) double layers. Stochastic heating of electrons does not yet play a significant role in the discharge under

these conditions. The ionization peak, corresponding to the third double layer, is also missing. At a voltage of 500 V (see Figure 9), peaks of the ionization rate appear due to stochastic heating and the formation of the third double layer (DL_3). Their intensity increases rapidly with the increase of the RF voltage amplitude, and at the maximum voltage of 1000 V considered by us, the intensities of all 4 peaks (StH , DL_1 , DL_2 , DL_3) become almost the same. That is, during the half of the RF period, the discharge is supported by 4 bursts of ionization in different parts of the gap between the electrodes, which, with some overlap in time, take place alternately $StH \rightarrow DL_1 \rightarrow DL_2 \rightarrow DL_3$.

Let's consider this procedure in more detail for the RF voltage amplitude of 1000 V. Figure 11 shows the axial profiles of the ionization and attachment rates for several moments of the RF period. At the initial moment, when the right electrode is a temporary anode and electron flow enters it, we see the presence of a peak near the electrode itself, which corresponds to the third double layer DL_3 . It is in this region that the ionization process occurs faster than the attachment. In other parts of the discharge, where the electrons are present (plasma volume and part of the right near-electrode layer), electron losses prevail. Next, the sign of the potential on the right electrode changes, it becomes a temporary cathode. The ionization rate for some time becomes small compared to the attachment rate ($t/T = 0.16$). Next, RF potential on the right electrode increases, the thickness of the right sheath increases, and at $t/T = 0.29$, the StH peak of stochastic electron heating is visible, and the passive DL_1 and active DL_2 double layers begin to form. Over time, the intensities of these three peaks increase, and at $t/T = 0.35$, when the RF current amplitude reaches a maximum, the ionization rate in the entire interval significantly exceeds the electron loss rate due to attachment. At $t/T > 0.4$, the peak of stochastic heating practically disappears, but the peak of the ionization rate appears near the left electrode (temporary anode) due to the formation of the third double layer DL_3 , which becomes dominant by the end of the half-period $t/T = 0.5$.

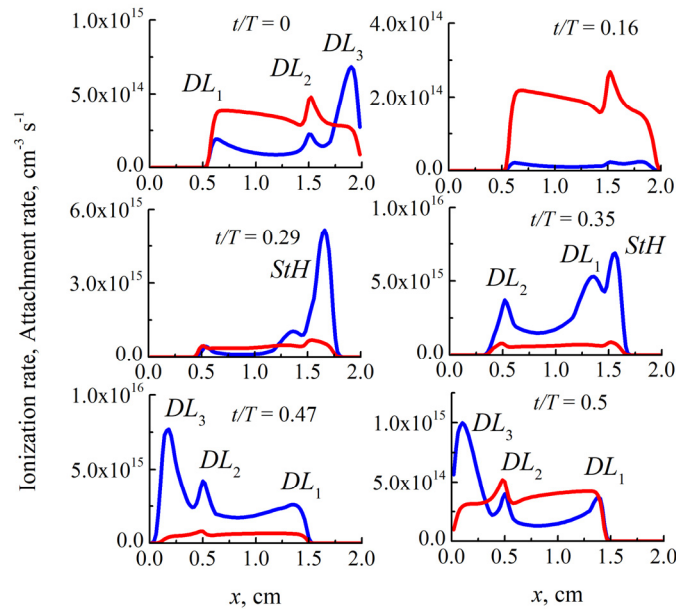


Figure 11. Axial profile of ionization (blue lines) and attachment (red lines) rates for different moments of the RF period t/T .
 $p = 1$ Torr, $f = 13.56$ MHz, $d = 2$ cm, $U_{rf} = 1000$ V

Next, we will consider ionization processes in a wide range of carbon dioxide pressures. The corresponding space-time dependences of the ionization rate are shown in Fig. 12 for the RF voltage amplitude of 1000 V. At a low pressure of 0.1 Torr, one broad peak of the ionization rate is observed during half of the RF period. To find out its nature, we will additionally analyze the axial profiles of reduced electric field strength E/p , shown in Fig. 13. From this figure, we can see that the ionization peak appeared as a result of the simultaneous action of stochastic heating and additional heating of electrons by the RF electric field in the plasma volume. Double layers are not observed under these conditions. When the gas pressure increases to 0.2 Torr, the ionization rate during half of the RF period has two maxima: first, stochastic heating occurs, and after $t/T > 0.25$, a wide double layer is formed, occupying most of the left near-electrode sheath. It is the same third, auxiliary double layer, which we talked about above.

At a gas pressure of 0.5 Torr, the peak of the active double layer is added to the ionization peaks of stochastic heating, and the third double layer, which is located near the boundary of the near-electrode sheath, while the passive double layer is still missing. It begins to appear at a gas pressure of 0.75 Torr and above. The peaks of the ionization rate for a carbon dioxide pressure of 1 Torr are shown in Fig. 10, and we found that at this pressure, all three double layers and stochastic heating are observed during half of the RF period. With a further increase in pressure to 1.5 Torr, the peak of stochastic heating weakens significantly, and the peak of the third double layer also becomes significantly weaker. In the case of a high gas pressure of 9.9 Torr, the peak of the active double layer dominates, the peak of the passive double layer is approximately twice as large, and we also see a constant level of ionization in the RF electric field in the plasma bulk.

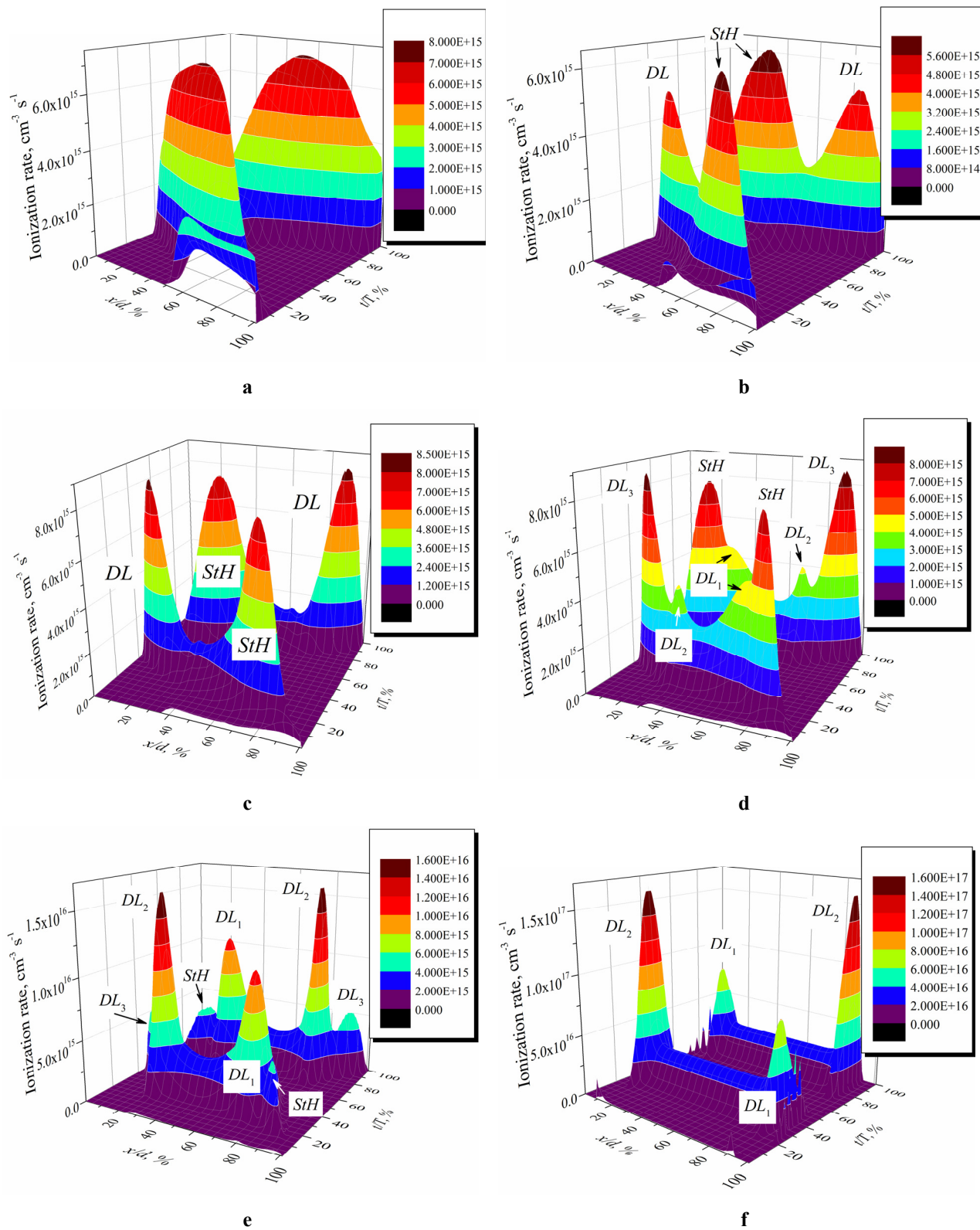


Figure 12. Space-time dependence of the ionization rate for different values of the gas pressure. $f = 13.56$ MHz, $d = 2$ cm, $U_{rf} = 1000$ V: a) 0.1 Torr; b) 0.2 Torr; c) 0.5 Torr; d) 0.75 Torr; e) 1.5 Torr; f) 9.9 Torr

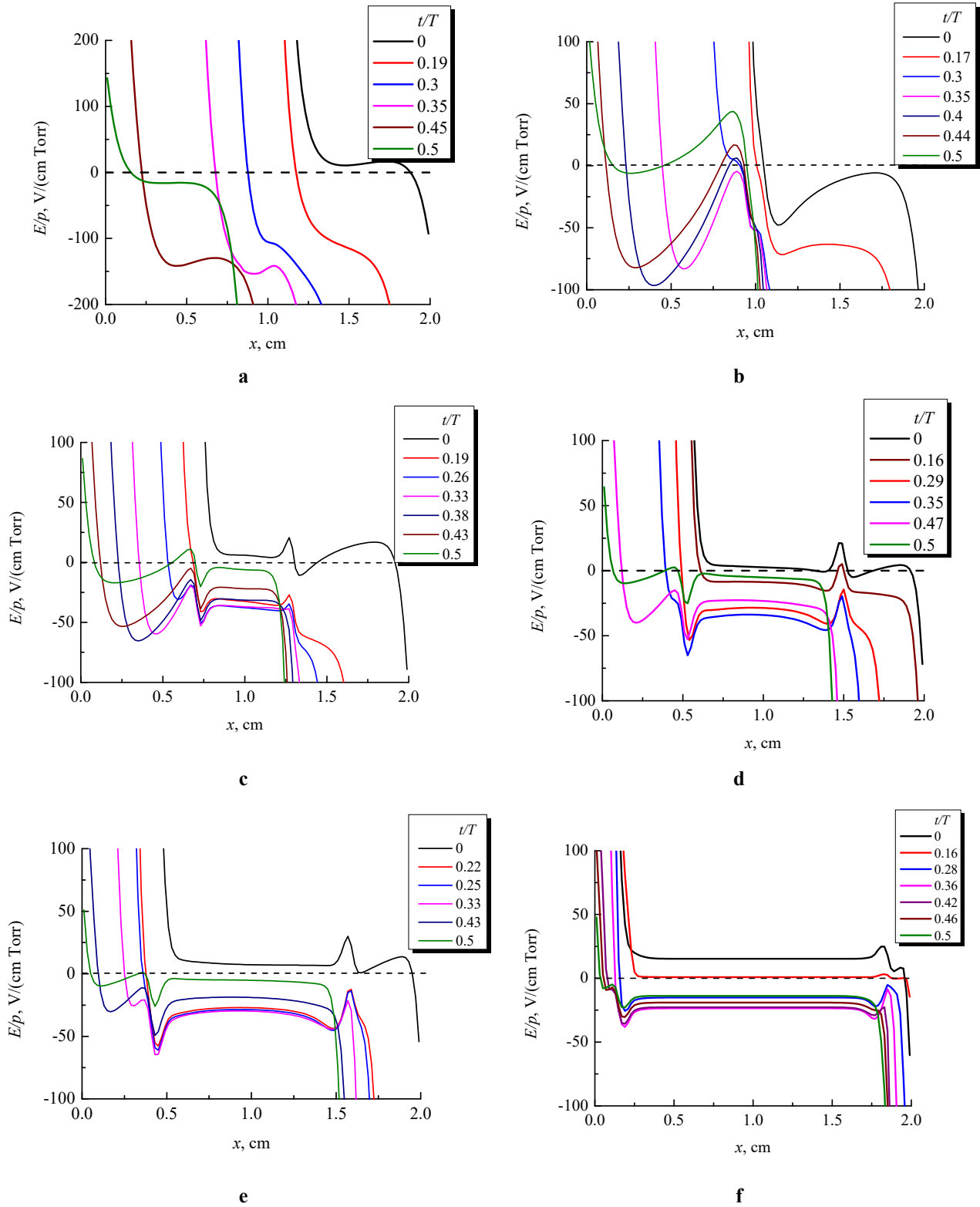


Figure 13. Axial profiles of the reduced electric field strength E/p at different moments of the RF period for different values of the gas pressure. $f = 13.56$ MHz, $d = 2$ cm, $U_{rf} = 1000$ V: a) 0.1 Torr; b) 0.2 Torr; c) 0.5 Torr; d) 1 Torr; e) 1.5 Torr; f) 9.9 Torr

As it follows from the above results, there is a narrow range of conditions under which 4 intensive ionization sources, stochastic heating, and 3 double layers (passive, active, and auxiliary) can participate in the discharge. This phenomenon is most clearly observed $p = 1 \pm 0.05$ Torr, $f = 13.56$ MHz and $d = 2$ cm at high RF voltages $U_{rf} = 500\text{--}1000$ V. For these conditions, $pd = 2$ Torr cm and $fd = 27.12$ MHz cm.

In [91], it was shown that RF gas breakdown and, in general, processes in RF capacitive discharge are controlled by the similarity law

$$U_{rf} = \psi\left(pd, fd, \frac{d}{R}\right),$$

where R is the radius of the discharge tube. Further analysis of the similarity law was carried out in papers [92–94].

Let's find out whether the presence of 4 intense ionization peaks will be observed at other distances between the electrodes, RF field frequencies, and gas pressure values. We will conduct the analysis for fixed values of the similarity parameters $pd = 2$ Torr cm and $fd = 27.12$ MHz cm. That is, after changing the frequency of the RF electric field, we must adjust the values of the distance between the electrodes and the gas pressure accordingly. For example, at a frequency of 3.89 MHz, the distance should be equal to 8 cm (to maintain $fd = 27.12$ MHz cm). Then the gas pressure should be 0.25 Torr (for $pd = 2$ Torr cm). We will do the same for other combinations of f , d and p . The calculation results presented in Fig. 14 show that at fixed values of the similarity parameters $pd = 2$ Torr cm and $fd = 27.12$ MHz cm, at least in the frequency range $f = 3.89\text{--}67.8$ MHz, 4 intense ionization peaks are observed. That is, our calculations using the SIGLO-rf code and the similarity law allow us to predict the behavior of ionization processes in a radio-frequency capacitive discharge.

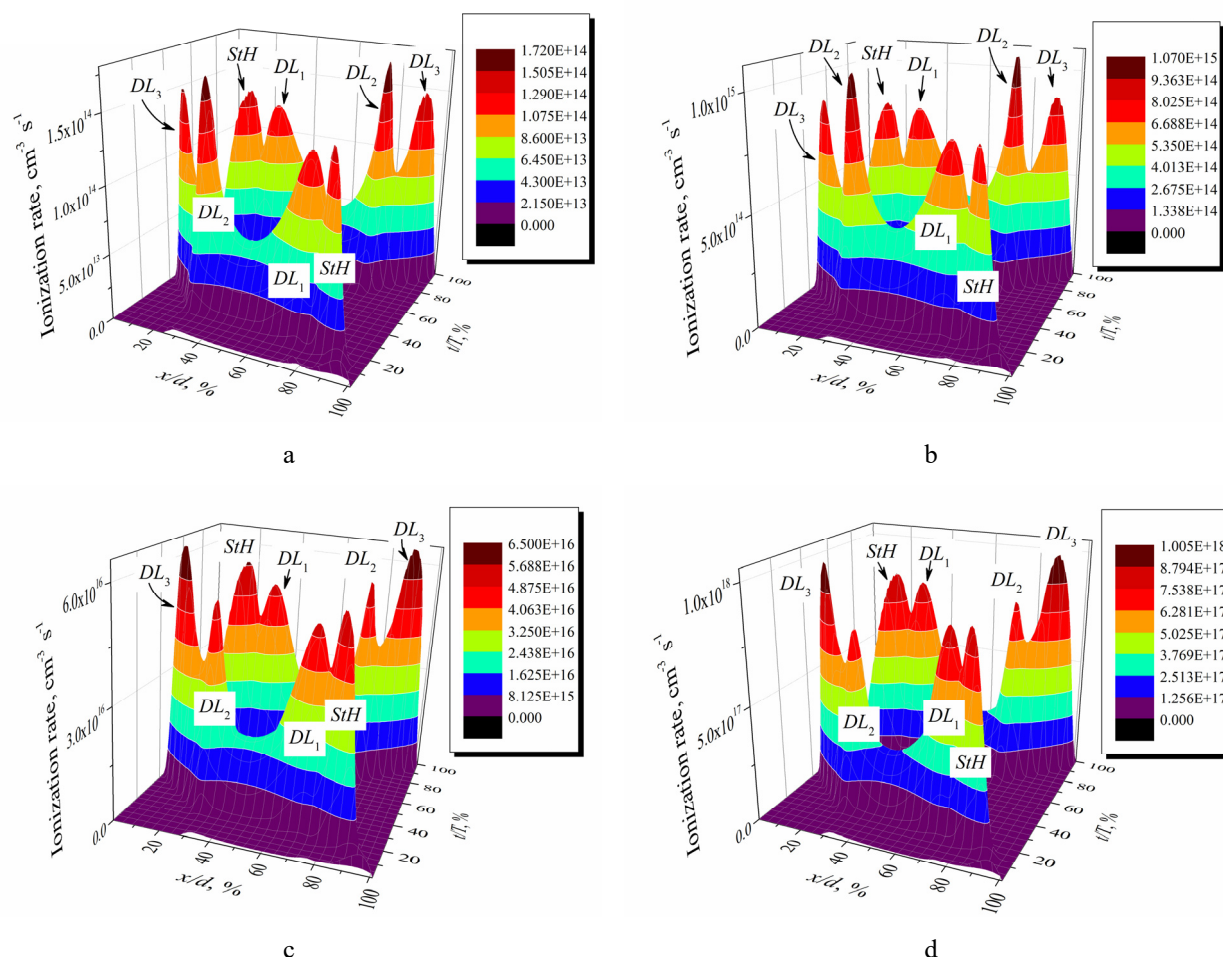


Figure 14. Space-time dependence of the ionization rate. $U_{rf} = 1000$ V:

- a) $f = 3.89$ MHz, $d = 8$ cm, $p = 0.25$ Torr; b) $f = 6.78$ MHz, $d = 4$ cm, $p = 0.5$ Torr; c) $f = 27.12$ MHz, $d = 1$ cm, $p = 2$ Torr; d) $f = 67.8$ MHz, $d = 0.04$ cm, $p = 5$ Torr

CONCLUSIONS

In this paper, the time-averaged and spatio-temporal profiles of the parameters of the RF capacitive discharge in carbon dioxide were investigated using the one-dimensional fluid code SIGLO-rf, which numerically calculates the balance equation (continuity equation) of electrons and each of the ion species (positive and negative), the electron energy

balance equation, and Poisson's equation for the electric potential. The processes of ionization bearing of electrons and positive ions, attachment of electrons to gas molecules, their detachment from negative ions, as well as processes of recombination of positive ions with electrons and negative ions are taken into account. Processes of ion-induced electron emission from the electrode surface are ignored, which limits the applicability of the code only to the low-current mode of RF capacitive discharge.

With the help of this SIGLO-rf code, the averaged over the RF period axial profiles of the densities of electrons, positive and negative ions, as well as the potential and electric field strength, were calculated in carbon dioxide. Most of the results were obtained for the distance between the electrodes $d = 2$ cm and RF frequency $f = 13.56$ MHz, but additional calculations were also carried out at $d = 0.04\text{--}8$ cm and $f = 3.89\text{--}67.8$ MHz. In the RF discharge in CO_2 , the quasi-neutral plasma consists of electrons and positive ions, and as a result of the process of dissociative attachment of electrons to gas molecules, negative ions of atomic oxygen appear. Their density in a quasi-neutral plasma is about ten times higher than the electron density. These negative ions are retained in the plasma volume and reduce the average potential of the plasma (compared to plasma in argon).

The spatio-temporal dynamics of electron density, potential and electric field strength, as well as ionization and attachment rates in RF capacitive discharge were also studied. It is shown that in the RF discharge in CO_2 , to ensure the balance of positive and negative charges that escape to the electrodes during the RF period, as well as to maintain quasi-neutrality in the regions filled with plasma, near the boundary of the sheaths, passive and active double layers are formed. In these double layers, thanks to the increased electric field, gas molecules are intensively ionized by electrons. At the same time, during the first half of the RF period, three bursts of ionization are observed in the RF discharge in CO_2 , which correspond to stochastic heating in one layer and the formation of double layers. This process is repeated in the reverse direction in the second half of the RF period.

It is shown that under certain conditions, $pd = 2$ Torr cm and $fd = 27.12$ MHz cm, even 4 ionization peaks can be observed during half of the RF period: resulting from stochastic heating, as well as the passive, active and auxiliary double layers. The auxiliary double layer occurs inside the near-electrode sheath near the surface of the temporary anode and contributes to bringing electrons to its surface. The simultaneous presence of 4 peaks was verified by calculations in a wide range of distances between electrodes, values of carbon dioxide pressure, and RF frequencies.

Acknowledgment

This work was supported by the National Research Foundation of Ukraine in the framework of the project 2021.01/0204.

ORCID

✉ V. Lisovskiy, <https://orcid.org/0000-0002-6339-4516>; ✉ S. Dudin, <https://orcid.org/0000-0001-9161-4654>
✉ V. Yegorenkov, <https://orcid.org/0000-0002-7252-3711>

REFERENCES

- [1] A. Lieberman, and A.J. Lichtenberg, *Principles of Plasma Discharges and Materials Processing*, 2nd ed. (Wiley, Hoboken, USA, 2005). <https://doi.org/10.1002/0471724254>
- [2] Yu.P. Raizer, M.N. Shneider, and N.A. Yatsenko, *Radio-frequency Capacitive Discharges* (CRC Press, Boca Raton, FL, 1995).
- [3] J. Reece Roth, *Industrial Plasma Engineering. vol. 2: Applications to Nonthermal Plasma Processing* (Bristol, IOP Publishing, 2001).
- [4] P. Chabert, and N. Braithwaite, *Physics of Radio-Frequency Plasmas* (Cambridge University Press, Cambridge, 2011).
- [5] M. Keidar, and I. Beilis, *Plasma Engineering* (Academic Press, London, 2018).
- [6] G. Colonna, and A. D'Angola, *Plasma Modeling: Methods and applications* (IOP Publishing, Bristol, 2022).
- [7] J.F. Friedrich, and J. Meichsner, *Nonthermal Plasmas for Materials Processing: Polymer Surface Modification and Plasma Polymerization* (Wiley-Scrivener, Hoboken, 2022).
- [8] L. Bardos, and H. Barankova, *Microwave Plasma Sources and Methods in Processing Technology* (Hoboken, Wiley-IEEE Press, 2022).
- [9] T. Shao, and Ch. Zhang, editors, *Pulsed Discharge Plasmas: Characteristics and Applications* (Springer, Singapore, 2023).
- [10] Ph. Belenguer, and J.P. Boeuf, *Physical Review A*, **41**, 4447 (1990), <https://doi.org/10.1103/PhysRevA.41.4447>
- [11] V.A. Godyak, R.B. Piejak, and B.M. Alexandrovich, *IEEE Transactions on Plasma Science*, **19**, 660 (1991). <https://doi.org/10.1109/27.90309>
- [12] V.A. Lisovskii, *Technical Physics Letters*, **24**, 308 (1998). <https://doi.org/10.1134/1.1262093>
- [13] V. Lisovskiy, J.-P. Booth, S. Martins, K. Landry, D. Douai, and V. Cassagne, *Europhysics Letters* **71**, 407 (2005). <https://doi.org/10.1209/epl/i2005-10108-1>
- [14] V. Lisovskiy, A. Minenkov, S. Dudin, S. Bogatyrenko, P. Platonov, and V. Yegorenkov, *ACS Omega* **7**, 47941 (2022). <https://doi.org/10.1021/acsomega.2c05846>
- [15] S.Y. Moon, J.K. Rhee, D.B. Kim, and W. Choe, *Physics of Plasmas*, **13**, 033502 (2006), <https://doi.org/10.1063/1.2177590>
- [16] V. Lisovskiy, J.-P. Booth, K. Landry, D. Douai, V. Cassagne, and V. Yegorenkov, *J. Phys. D: Appl. Phys.* **40**, 6631 (2007). <https://doi.org/10.1088/0022-3727/40/21/023>
- [17] V. Lisovskiy, J.-P. Booth, J. Jolly, S. Martins, K. Landry, D. Douai, V. Cassagne, and V. Yegorenkov, *J. Phys. D: Appl. Phys.* **40**, 6989 (2007), <https://doi.org/10.1088/0022-3727/40/22/020>
- [18] V. Lisovskiy, V. Yegorenkov, E. Artushenko, J.-P. Booth, S. Martins, K. Landry, D. Douai, and V. Cassagne, *Plasma Sources Sci. Technol.* **22**, 015018 (2013). <https://doi.org/10.1088/0963-0252/22/1/015018>
- [19] V. Godyak, *Phys. Plasmas*, **27**, 013504 (2020). <https://doi.org/10.1063/1.5122957>

- [20] M.A. Lieberman, IEEE Trans. Plasma Sci. **17**, 338 (1989). <https://doi.org/10.1109/27.24645>
- [21] M.A. Lieberman, IEEE Trans. Plasma Sci. **16**, 638 (1988). <https://doi.org/10.1109/27.16552>
- [22] A.J. Lichtenberg, V. Vahedi, M.A. Lieberman, and T. Rognlien, J. Appl. Phys. **75**, 2339 (1994). <https://doi.org/10.1063/1.356252>
- [23] F. Hamaoka, T. Yagisawa, and T. Makabe, J. Phys: Conf. Series **86**, 012018 (2007). <https://doi.org/10.1088/1742-6596/86/1/012018>
- [24] V.I. Kolobov, R.R. Arslanbekov, D. Levko, and V.A. Godyak, J. Phys. D: Appl. Phys. **53**, 25LT01 (2020). <https://doi.org/10.1088/1361-6463/ab7ca0>
- [25] J.P. Verboncoeur, M. Alves, V. Vahedi, and C. Birdsall, Simultaneous potential and circuit solution for 1D bounded plasma particle simulation codes J. Comput. Phys. **104**, 321 (1993). <https://doi.org/10.1006/jcph.1993.1034>
- [26] V. Vahedi, C.K. Birdsall, M.A. Lieberman, G. DiPeso, and T.D. Rognlien, Plasma Sources Sci. Technol. **2**, 273 (1993). <https://doi.org/10.1088/0963-0252/2/4/007>
- [27] T. Lafleur, P. Chabert, and J.P. Booth, Plasma Sources Sci. Technol. **23**, 035010 (2014). <https://doi.org/10.1088/0963-0252/23/3/035010>
- [28] E. Kawamura, M.A. Lieberman, A.J. Lichtenberg, and P. Chabert, J. Vac. Sci. Technol. A, **38**, 023003 (2020). <https://doi.org/10.1116/1.5135575>
- [29] J.T. Gudmundsson, J. Krek, D.-Q. Wen, E. Kawamura, and M.A. Lieberman, Plasma Sources Sci. Technol. **30**, 125011 (2021). <https://doi.org/10.1088/1361-6595/ac3ba1>
- [30] Z. Donkó, Plasma Sources Sci. Technol. **20**, 024001 (2011). <https://doi.org/10.1088/0963-0252/20/2/024001>
- [31] J. Schulze, E. Schüngel, A. Derzsi, I. Korolov, Th. Mussenbrock, and Z. Donkó, IEEE Trans. Plasma Sci. **42**, 2780 (2014). <https://doi.org/10.1109/TPS.2014.2306265>
- [32] M. Vass, S. Wilczek, T. Lafleur, R. P. Brinkmann, Z. Donko, and J. Schulze, Plasma Sources Sci. Technol. **29**, 085014 (2020). <https://doi.org/10.1088/1361-6595/aba111>
- [33] D.A. Schulenberg, I. Korolov, Z. Donko, A. Derzsi, and J. Schulze, Plasma Sources Sci. Technol. **30**, 105003 (2021). <https://doi.org/10.1088/1361-6595/ac2222>
- [34] D.-Q. Wen, J. Krek, J. T. Gudmundsson, E. Kawamura, M. A. Lieberman, P. Zhang, and J. P. Verboncoeur, Plasma Sources Sci. Technol. **32**, 064001 (2023). <https://doi.org/10.1088/1361-6595/acd6b4>
- [35] A. Derzsi, B. Horváth, Z. Donkó, and J. Schulze, Plasma Sources Sci. Technol. **29**, 074001 (2020). <https://doi.org/10.1088/1361-6595/ab9156>
- [36] S. Rauf, Plasma Sources Sci. Technol. **29**, 095019 (2020). <https://doi.org/10.1088/1361-6595/abac4a>
- [37] L. Wang, P. Hartmann, Z. Donkó, Y.-H. Song, and J. Schulze, Plasma Sources Sci. Technol. **30**, 085011 (2021). <https://doi.org/10.1088/1361-6595/abf206>
- [38] L. Wang, P. Hartmann, Z. Donkó, Y.-H. Song, and J. Schulze, J. Vac. Sci. Technol. A **39**, 063004 (2021). <https://doi.org/10.1116/6.0001327>
- [39] S. Sharma, S. Patil, S. Sengupta, A. Sen, A. Khrabrov, and I. Kaganovich, Phys. Plasmas, **29**, 063501 (2022). <https://doi.org/10.1063/5.0094409>
- [40] A. Picard, G. Turban, and B. Grolleau, J. Phys. D: Appl. Phys. **19**, 991 (1986). <https://doi.org/10.1088/0022-3727/19/6/014>
- [41] N. Nakano, N. Shimura, Z. Lj. Petrovic, and T. Makabe, Phys. Rev. E, **49**, 4455 (1994). <https://doi.org/10.1103/PhysRevE.49.4455>
- [42] Y.T. Lee, M.A. Lieberman, A.J. Lichtenberg, F. Bose, H. Baltes, and R. Patrick, J. Vac. Sci. Technol. A: Vacuum, Surfaces and Films, **15**, 113 (1997). <https://doi.org/https://doi.org/1116/1.580452>
- [43] M. Shibata, T. Makabe, and N. Nakano, Jpn. J. Appl. Phys. **37**, 4182 (1998). <https://doi.org/10.1143/JJAP.37.4182>
- [44] V.A. Lisovskiy and V.D. Yegorenkov, Vacuum, **80**, 458 (2006). <https://doi.org/10.1016/j.vacuum.2005.07.038>
- [45] J. Schulze, A. Derzsi, K. Dittmann, T. Hemke, J. Meichsner, and Z. Donkó, Phys. Rev. Lett. **107**, 275001 (2011). <https://doi.org/10.1103/PHYSREVLETT.107.275001>
- [46] E. Kawamura, A.J. Lichtenberg, and M.A. Lieberman, J. Phys. D: Appl. Phys. **45**, 495201 (2012). <https://doi.org/10.1088/0022-3727/45/49/495201>
- [47] V. Lisovskiy, and V. Yegorenkov, EPL, **99**, 35002 (2012). <https://doi.org/10.1209/0295-5075/99/35002>
- [48] A. Proto, and J.T. Gudmundsson, J. Appl. Phys. **128**, 113302 (2020). <https://doi.org/10.1063/5.0019340>
- [49] A. Proto, and J.T. Gudmundsson, Plasma Sources Sci. Technol. **30**, 065009 (2021). <https://doi.org/10.1088/1361-6595/abef1d>
- [50] A. Derzsi, P. Hartmann, M. Vass, B. Horváth, M. Gyulai, I. Korolov, J. Schulze, and Z. Donko, Plasma Sources Sci. Technol. **31**, 085009 (2022). <https://doi.org/10.1088/1361-6595/ac7b45>
- [51] C. Harvey, N. Sirse, C. Gaman, and A. R. Ellingboe, Phys. Plasmas, **27**, 110701 (2020). <https://doi.org/10.1063/5.0022844>
- [52] A. Derzsi, M. Vass, R. Masheyeva, B. Horváth, Z. Donkó, and P. Hartmann, Plasma Sources Sci. Technol. **33**, 025005 (2024). <https://doi.org/10.1088/1361-6595/ad1fd5>
- [53] R. Masheyeva, M. Vass, X.-K. Wang, Y.-X. Liu, A. Derzsi, P. Hartmann, J. Schulze, and Z. Donkó, Plasma Sources Sci. Technol. **33**, 045019 (2024). <https://doi.org/10.1088/1361-6595/ad3c69>
- [54] R.A. Gottscho, Phys. Rev. A **36**, 2233 (1987). <https://doi.org/10.1103/PhysRevA.36.2233>
- [55] R.A. Gottscho, and C.E. Gaebe, IEEE Trans. Plasma Sci. **PS-14**, 92 (1986). <https://doi.org/10.1109/TPS.1986.4316511>
- [56] J.-P. Boeuf, Phys. Rev. A, **36**, 2782 (1987). <https://doi.org/10.1103/PhysRevA.36.2782>
- [57] J. P. Boeuf, and P. Belenguer, in *Nonequilibrium Processes in Partially Ionized Gases*, edited by M. Capitelli and J. N. Bardsley (Springer, New York, 1990). pp. 155–186. https://doi.org/10.1007/978-1-4615-3780-9_9
- [58] J.P. Boeuf, and L.C. Pitchford, Phys. Rev. E, **51**, 1376 (1995). <https://doi.org/10.1103/PhysRevE.51.1376>
- [59] P. Vitruk, H. Baker, and D. Hall, IEEE J. Quantum Electronics, **30**, 1623 (1994). <https://doi.org/10.1109/3.299494>
- [60] G.A.J. Markille, J.J. Baker, J.G. Betterton, and D.R. Hall, IEEE J. Quantum Electronics, **35**, 1134 (1999). <https://doi.org/10.1109/3.777212>

- [61] R. Engelbrecht, R. Schulz, G. Seibert, J. Hagen, and L.-P. Schmidt, *Frequenz*, **59**, 154 (2005). <https://doi.org/10.1515/freq.2005.59.5-6.154>
- [62] O. Svelto, *Principles of lasers*, (Springer, New York, 2009). 604 p.
- [63] A. Bogaerts, T. Kozak, K. van Laer, and R. Snoeckx, *Faraday Discuss.* **183**, 217 (2015). <https://doi.org/10.1039/C5FD00053J>
- [64] T. Kozak, and A. Bogaerts, *Plasma Sources Sci. Technol.* **24**, 015024 (2014). <https://doi.org/10.1088/0963-0252/24/1/015024>
- [65] R. Snoeckx, and A. Bogaerts, *Chem. Soc. Rev.* **46**, 5805 (2017). <https://doi.org/10.1039/C6CS00066E>
- [66] A. Bogaerts, and G. Centi, *Frontiers in Energy Research*, **8**, 111 (2020). <https://doi.org/10.3389/fenrg.2020.00111>
- [67] G. Chen, R. Snyders, and N. Britun, *J. CO₂ Utilization*, **49**, 101557 (2021). <https://doi.org/10.1016/j.jcou.2021.101557>
- [68] S. Dudin, V. Lisovskiy, P. Platonov, and S. Rezunenko, *Problems of Atomic Science and Technology*, **6**(142), 84 (2022). https://vant.kipt.kharkov.ua/ARTICLE/VANT_2022_6/article_2022_6_84.pdf
- [69] V.A. Lisovskiy, S.V. Dudin, P.P. Platonov, and V.D. Yegorenkov, *East European J. Phys.* (4), 152 (2021). <https://doi.org/10.26565/2312-4334-2021-4-20>
- [70] V.A. Lisovskiy, S.V. Dudin, P.P. Platonov, and V.D. Yegorenkov, *Problems of atomic science and technology*, **6**(130), 179 (2020). https://vant.kipt.kharkov.ua/ARTICLE/VANT_2020_6/article_2020_6_179.pdf
- [71] A.S. Morillo-Candas, V. Guerra, and O. Guaitella, *J. Phys. Chem. C*, **124**, 17459 (2020). <https://doi.org/10.1021/acs.jpcc.0c03354>
- [72] R. Vertongen, G. Trenchev, R. Van Loenhout, and A. Bogaerts, *J. CO₂ Utilization*, **66**, 102252 (2022). <https://doi.org/10.1016/j.jcou.2022.102252>
- [73] Q. Fu, Y. Wang, and Zh. Chang, *J. CO₂ Utilization*, **70**, 102430 (2023). <https://doi.org/10.1016/j.jcou.2023.102430>
- [74] E.R. Mercer, S. Van Alphen, C.F.A.M. van Deursen, T.W.H. Righart, W.A. Bongers, R. Snyders, A. Bogaerts, *et al.*, *Fuel*, **334**, 126734 (2023). <https://doi.org/10.1016/j.fuel.2022.126734>
- [75] S. Kelly, E. Mercer, Y. Gorbanev, I. Fedirchuk, C. Verheyen, K. Werner, P. Pullumbi, A. Cowley, and A. Bogaerts, *J. CO₂ Utilization*, **80**, 102668 (2024). <https://doi.org/10.1016/j.jcou.2024.102668>
- [76] Y. Long, X. Wang, H. Zhang, K. Wang, W.-L. Ong, A. Bogaerts, K. Li, *et al.*, *JACS Au*, **4**, 7 2462 (2024). <https://doi.org/10.1021/jacsau.4c00153>
- [77] G.J.M. Hagelaar and L.C. Pitchford, *Plasma Sources Sci. Technol.* **14**, 722 (2005). <https://doi.org/10.1088/0963-0252/14/4/011>
- [78] L.C. Pitchford, L.L. Alves, K. Bartschat, S.F. Biagi, M.C. Bordage *et al.*, *Plasma Process. Polym.* **14**, 1600098 (2017). <https://doi.org/10.1002/ppap.201600098>
- [79] Y. Itikawa, *J. Phys. Chem. Reference Data*, **31**, 749 (2002). <https://doi.org/10.1063/1.1481879>
- [80] V.A. Lisovskiy, S.V. Dudin, P.P. Platonov, and V.D. Yegorenkov, *Physica Scripta*, **98**, 025601 (2023). <https://doi.org/10.1088/1402-4896/acae48>
- [81] H.W. Ellis, R.Y. Pai, E.W. McDaniel, E.A. Mason, and L.A. Viehland, *Atomic Data and Nuclear Data Tables*, **17**, 177 (1976). [https://doi.org/10.1016/0092-640X\(76\)90001-2](https://doi.org/10.1016/0092-640X(76)90001-2)
- [82] P. Coxon, and J. Moruzzi, *J. Phys. Colloques*, **40**, 117 (1979). <https://doi.org/10.1051/jphyscol:1979758>
- [83] E.W. McDaniel, and H. Crane, *Rev. Sci. Instruments*, **28**, 684 (1957). <https://doi.org/10.1063/1.1715976>
- [84] W.L. Nighan, and W.J. Wiegand, *Phys. Rev. A*, **10**, 922 (1974). <https://doi.org/10.1103/PhysRevA.10.922>
- [85] C.S. Weller, and M.A. Biondi, *Phys. Rev. Lett.* **19**, 59 (1967). <https://doi.org/10.1103/PhysRevLett.19.59>
- [86] Yu.P. Raizer, *Gas discharge physics*, (Springer, Berlin, 1991).
- [87] T.D. Fansler, L.M. ColonnaRomano, and R.N. Varney, *J. Chem. Phys.* **66**, 3246 (1977). <https://doi.org/10.1063/1.434300>
- [88] V. Lisovskiy, S. Dudin, A. Shakhnazarian, P. Platonov, and V. Yegorenkov, *Problems of Atomic Science and Technology*, **4**(129), (2023). https://vant.kipt.kharkov.ua/ARTICLE/VANT_2023_4/article_2023_4_129.pdf
- [89] V.A. Lisovskiy, S.V. Dudin, M.M. Vusyk, R.O. Osmayev, V.D. Yegorenkov, and P.P. Platonov, *Problems of Atomic Science and Technology*, 186, (2023). https://vant.kipt.kharkov.ua/ARTICLE/VANT_2023_1/article_2023_1_86.pdf
- [90] P. Capezzuto, F. Cramarossa, R. D'Agostino, and E. Molinari, *J. Phys. Chem.* **80**, 882 (1976). <https://doi.org/10.1021/j100549a024>
- [91] V. Lisovskiy, J.P. Booth, K. Landry, D. Douai, V. Cassagne, and V. Yegorenkov, *Europhys. Lett.* **82**, 15001 (2008). <https://doi.org/10.1209/0295-5075/82/15001>
- [92] Y. Fu, H. Wang, and X. Wang, *Rev. Modern Plasma Phys.* **7**, 10 (2023). <https://doi.org/10.1007/s41614-022-00112-1>
- [93] Y. Fu, B. Zheng, P. Zhang, Q.H. Fan, J.P. Verboncoeur, and X. Wang, *Phys. Plasmas*, **27**, 113501 (2020). <https://doi.org/10.1063/5.0022788>
- [94] [Y. Fu, B. Zheng, D.-Q. Wen, P. Zhang, Q.H. Fan, and J.P. Verboncoeur, *Appl. Phys. Lett.* **117**, 204101 (2020). <https://doi.org/10.1063/5.0029518>

ЧИСЕЛЬНЕ МОДЕЛЮВАННЯ ДИНАМІКИ ВЧ ЄМНІСНОГО РОЗРЯДУ У ВУГЛЕКИСЛОМУ ГАЗІ

В. Лісовський, С. Дудін, А. Шахназарян, П. Платонов, В. Єгоренков

Харківський національний університет імені В.Н. Каразіна, майдан Свободи, 4, Харків, 61022, Україна

У цій роботі одновимірний гідродинамічний код SIGLO-rg було використано для дослідження внутрішніх параметрів ВЧ ємнісного розряду у вуглекислому газі. Проведено моделювання середніх за часом та просторово-часових профілів параметрів розряду. Для цього чисельно розв'язано рівняння балансу концентрації для кожного з видів заряджених частинок та рівняння балансу енергії електронів, які були доповнені також рівнянням Пуассона для електричного потенціалу. За допомогою цього коду SIGLO-rg в діапазоні відстаней між електродами $d = 0,04 - 8$ см, частот ВЧ електричного поля $f = 3,89 - 67,8$ МГц та значень тиску вуглекислого газу $p = 0,1 - 9,9$ Торр розраховано середні за ВЧ період осові профілі густини електронів, позитивних та негативних іонів, а також потенціалу та напруженості електричного поля. Показано, що розрядна плазма в CO₂ містить електрони, позитивні іони, а також негативні іони. Вони утворилися при дисоціативному прилипанні електронів до молекул CO₂ й є негативними іонами атомарного кисню. Зазвичай плазма ВЧ ємнісного розряду є фактично іон-іонною, тому що концентрація вільних електронів у декілька десятків разів менша за концентрацію негативних іонів. Негативні іони накопичуються у плазмі завдяки утриманню в середній за часом потенціальній ямі, що призводить до

зменшення потенціалу плазми. Дослідження просторово-часової динаміки параметрів плазми (густини електронів, потенціалу та напруженості електричного поля, а також швидкостей іонізації та прилипання) у ВЧ ємнісному розряді в CO_2 показали, що протягом однієї половини ВЧ періоду зазвичай спостерігаються від 1 до 3 сплесків іонізації. Вони відповідають стохастичному нагріву у приелектродному шарі, що є у катодній фазі й межує з тимчасовим негативним електродом, та формуванню пасивного та активного подвійних шарів біля меж приелектродних шарів. Пасивний подвійний шар знаходиться біля межі приелектродного шару у катодній фазі й підтримує розрядну плазму. Активний шар формується біля межі приелектродного шару в анодній фазі й забезпечує баланс позитивного та негативного зарядів, що надходять в електрод протягом усього ВЧ періоду. З'ясовано, що при одночасному виконанні умов $pd = 2$ Торр см та $fd = 27,12$ МГц см протягом половини ВЧ періоду спостерігаються 4 інтенсивних іонізаційних піки: внаслідок стохастичного нагріву, а також формування пасивного, активного та додаткового (допоміжного) подвійних шарів. Додатковий подвійний шар сприяє підведенню електронів до поверхні тимчасового анода й виникає поблизу його поверхні всередині приелектродного шару. За допомогою закону подібності перевірено умови існування цих 4 піків іонізації в широкому діапазоні ВЧ частот f , значень тиску вуглекислого газу p та відстаней між електродами d .

Ключові слова: високочастотний ємнісний розряд; гідродинамічне моделювання; вуглекислий газ; швидкість іонізації; подвійні шари, негативні іони